Research Article | Vol. 10, No. 2 / 1 February 2020 / Optical Materials Express 282
Optical Materials EXPRESS

Tunable terahertz phase shifter based on dielectric artificial birefringence grating filled with polymer dispersed liquid crystal

XIN ZHANG,[1] FEI FAN,[1,2,3,*] CHUN-YUE ZHANG,[1] YUN-YUN JI,[1] XIANG-HUI WANG,[1] AND SHENG-JIANG CHANG[1,2]

[1]*Institute of Modern Optics, Nankai University, Tianjin 300350, China*
[2]*Tianjin Key Laboratory of Optoelectronic Sensor and Sensing Network Technology, Tianjin 300350, China*
[3]*State Key Laboratory of Applied Optics, Changchun Institute of Optics, Fine Mechanics and Physics, Chinese Academy of Sciences, Changchun 130033, China*
[*]*fanfei_gdz@126.com*

Abstract: An active terahertz (THz) anisotropic manipulation is based on a structure combined polymer dispersed liquid crystal (PDLC) with sub-wavelength dielectric gradient grating. In this structure, the PDLC works as an adjustable anisotropic material due to the change of the optical axis direction induced by applying a biased electric field, while the dielectric grating serves as an artificial high birefringence material. By using an appropriate design, the THz birefringence of this structure can be enhanced or offset under different biased voltages, and the phase shift curve of this structure becomes flatter than that of the pure PDLC cell due to the dispersion manipulation of the grating. Moreover, the experimental results fit with the simulative designing, demonstrating that the phase shift of the structure can vary from π to 0 near 0.8 THz when the electric field increases from 0 to 80V, and this device realizes the function of polarization conversion as a tunable THz half-wave plate. This work exhibits potential applications in THz functional devices, such as actively controlled phase shifters and polarization convertors combined LC with artificial microstructure.

1. Introduction

Terahertz (THz) wave refers to the frequency ranged from 0.1 to 10 THz between microwave and infrared regime. In the past few decades, with the fairly great developments of THz science and technology, there are increasing attentions attached to THz functional devices, such as THz filters [1], modulators [2], phase shifters [3], polarization convertors [4], etc, showing large potential and wide application prospect in THz communication [5], imaging [6], sensing [7], and so on. Among these THz devices, phase shifters are undoubtedly essential components for controlling the phase retardation, polarization conversion, and wavefront modulation. However, the phase shifters based on natural uniaxial crystals, such as quartz and calcite, are limited in the THz wavelength due to their low birefringence and bulk structure.

Artificial microstructures, such as metamaterial and subwavelengh grating, can bring much higher artificial birefringence than that of natural crystals, and its dispersion can be engineered in the broadband frequency range. For instance, Wang *et al.* reported an ultrathin THz quarter-wave based on planar babinet-inverted metasurface [8], finally achieving a phase shift of 90° at 0.87 THz. Ke *et al.* proposed an efficient and broadband THz quarter-wave plate by designing double-stacked hyperbolic metamaterial waveguide arrays [9], eventually reaching $\pi/2$ over a wide spectral band ranged from 0.9 to 1.2 THz. Han *et al.* presented a THz quarter-wave plate based on a thin film metamaterial with double-layer split ring resonators, and experimentally confirmed a transmittance of 0.8 and an ellipticity of 0.99 at 0.98 THz [10]. However, these

#383058 https://doi.org/10.1364/OME.383058
Journal © 2020 Received 11 Nov 2019; revised 7 Dec 2019; accepted 14 Dec 2019; published 2 Jan 2020

Optical Materials EXPRESS

devices cannot be actively controlled by the external fields. It is an urgent demand to develop active THz phase shift devices covered tunable range from 0 to π rad.

Liquid crystals (LCs) have attracted wide attention in the development of tunable phase and polarization control devices thanks to their large optical anisotropy [11–13], which can be flexibly controlled by thermal, optical, electrical or magnetic field [14–16]. The optical properties of LCs in the THz regime have been extensively studied in recent years. For examples, Nico *et al.* reported the frequency and temperature dependent refractive index and absorption coefficient of 5CB, 6CB and 7CB under the terahertz time domain spectroscopy (THz-TDS) system [17]. Yang *et al.* presented an adjustable THz wave plate based on three different LCs (5CB, E7 and BNHR) [18], which can provide a relatively large birefringence. Among the different kinds of LCs, polymer dispersed liquid crystal (PDLC) impresses researchers with advantages of short response time, good surface pre-anchoring, and uniformity of dispersion in the polymer solvent, and its optical properties in the visible and THz band have been studied for further application of PDLC. Harbour *et al.* reported the optical birefringence and anisotropic scattering of PDLC [19]. Yo *et al.* reported the response time of PDLC with 4 ms in the THz frequency band [20]. Chang *et al.* demonstrated a THz tunable fishnet metamaterial using an electrically controlled PDLC matrix [21], obtaining a phase shift of 70° at 280 V. Despite with these advantages of LCs, there are also some other drawbacks, for examples, the ineffective initial surface anchoring, high driving voltage [22] and limited phase modulation range [23].

For further developments of THz devices, artificial microstructures, like metamaterials [24], metasurfaces [25], and sub-wavelength gratings [26], are introduced to combine with LC because of the easily engineered structures. Sasaki *et al.* proposed a 90 degrees-twisted nematic LC cell with subwavelength metallic gratings [26]. J.Wang *et al.* presented an electrically adjustable THz modulator based on LC and metamaterial with a large modulation depth beyond 90% and a low insertion loss below 0.5 dB [27]. L.Wang *et al.* reported a tunable THz metamaterial absorber integrated few-layer porous graphene with LC [28,29], demonstrating a tunable resonant frequency from 0.75 to 1 THz and an amplitude modulation of 80% corresponding to these frequencies at 10 V. Yang *et al.* designed a nematic LC (NLC)-based tunable THz plasmonic metamaterial [30], and experimentally demonstrated the amplitude modulation depth and insertion loss are about 96% and 1.19 dB at 0.42 THz, respectively, when the bias voltage applied to the NLC layer changes from 0 to 16 V. Such THz devices based on the frequency shift of resonance peak caused by the change of refractive index are mainly utilized as switches, filters, absorbers, and modulators, while there are merely a few reports on THz anisotropic devices that combine LC and microstructure to realize the polarization conversion, therefore still requiring further investigations in this area.

In this work, we proposed an electrically adjustable THz phase shifter based on a structure combined PDLC with a sub-wavelength dielectric grating. Here, the PDLC is used as a tunable anisotropic material due to the rotation of optical axis caused by biased electric field, and the grating acts as an anisotropic material with a fixed optical axis. By a suitable design, the anisotropy of this structure can be enhanced or eliminated at different biased voltages. Furthermore, we have experimentally verified the phase shift of this structure can change from π at 0 V to 0 at 80 V near 0.8 THz, implementing the function as a tunable THz half-wave plate, which shows a promising prospect in THz functional devices, like actively tunable phase shifters and polarization convertors.

2. Results and discussions

2.1. THz birefringence properties of PDLC

The PDLC used in the experiment was mixed of a polymer solvent named epoxy resin and a mixture of LCs called E7 by using the method of UV polymerization. The quality percentage of the epoxy resin in the PDLC is 30 wt%, and its refractive index is around 1.95 in the THz

Optical Materials EXPRESS

band. The refractive indices of E7 are $n_e = 1.78$ and $n_o = 1.58$, and the absorption coefficients of o-light and e-light of E7 at 0.8 THz are 15 cm^{-1} and 5 cm^{-1}, respectively [31]. First, we prepared a PDLC cell of 500 μm thickness, and made the initial anchoring process by applying ultraviolet (UV) light and the external magnetic field. As shown in Fig. 1(a), the LC molecules are randomly dispersed in the polymer solvent, and the orientation of the LC molecules is also random, thus the PDLC is isotropic in this case. Then the LC cell was irradiated by UV light of 365 nm wavelength and 8 mW/cm^2 for 5 mins, and meanwhile an external magnetic field of 70 mT was applied along x axis so as to orient the LC molecules. As shown in Fig. 1(b), after this process, many polymer-coated LC droplets with the size of the order of micrometer are formed in the polymer solvent, and the LC molecules in these droplets are aligned along the magnetic field direction. When the magnetic field is removed, the LC molecules are still regularly arranged along the original magnetic field direction due to the surface interaction with the droplets. Finally, we obtained the PDLC cell with the initial anchoring direction and a stable anisotropic state for a long time at room temperature. The anchoring direction of the optical axis of LC molecules is set along the x axis.

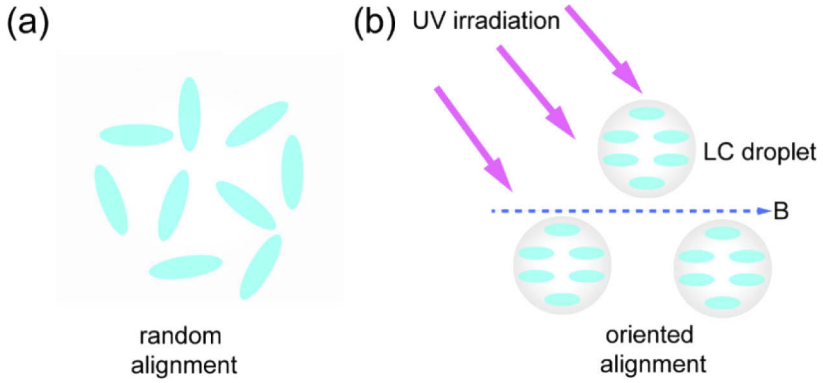

Fig. 1. Initial anchoring process of PDLC. (a) Schematic diagram showing the initial state of PDLC molecules with random alignments dispersed in the polymer solvent; (b) The state of PDLC molecules after being irradiated by the UV light and oriented by a magnetic field of 70 mT along the x axis.

The THz optical properties of PDLC were measured by the THz-TDS system shown in Fig. 2(a). In this system, the THz pulse is generated by a GaAs photoconductive antenna (PCA), which is excited by a Ti:sapphire laser with 80 fs duration of 80 MHz repetition rate working at 800 nm, and a ZnTe crystal is used for the electro-optical sampling detection. The polarizing direction of the incident linearly polarized (LP) THz wave is always along y axis. A THz polarizer is placed behind the sample to detect the polarization state of the output light. All of the experiments are performed at room temperature with the humidity of under 5%.

In the first step of the experiment, the polarizer in the THz-TDS system was fixed at 0° (the transmitting direction along y axis). Since the PDLC has been initially oriented, we set the angle between its optical axis direction (*i.e.* PDLC molecular orientation direction) and x axis as θ. Thus, we measured the time domain signal of o-light when we placed the PDLC cell as θ=0°. Then the PDLC cell was rotated to 90°, and at this time the optical axis of the PDLC was along the y axis (θ=90°), so the time domain signal of e-light was obtained. All the results are presented in Fig. 2(b).

After Fourier transform of the two signals above, the refractive index $n(\omega)$, extinction coefficient $\kappa(\omega)$, and absorption coefficient $\alpha(\omega)$ of o-light and e-light can be calculated by [3]

$$n(\omega) = 1 + \frac{\Delta\delta(\omega)c}{\omega d} \tag{1}$$

Optical Materials EXPRESS

$$\kappa(\omega) = \frac{-\ln\left(t(\omega)\frac{[n(\omega)+1]^2}{4n(\omega)}\right)c}{\omega d} \tag{2}$$

$$\alpha(\omega) = \frac{2\omega\kappa(\omega)}{c} \tag{3}$$

where c is the speed of light in vacuum, d denotes the thickness of the PDLC layer used in the experiment ($d = 500$ μm here), and ω is the circular frequency of THz waves. $\Delta\delta(\omega) = \Delta\delta_s - \Delta\delta_r$ and $t(\omega) = T_s/T_r$ are the phase difference and amplitude transmission between the sample and reference (*i.e.* blank cell), respectively. The intensity transmittance $I(\omega)=t(\omega)^2$. The intensity transmittance of *e*-light exhibited in Fig. 2(c) is over 80% due to a low absorption of lower than 5 cm^{-1} shown in Fig. 2(d), but the transmittance of *o*-light is lower than that of *e*-light because of a larger absorption loss with an absorption coefficient $\alpha(\omega) = 12\,cm^{-1}$ at 1 THz. As shown

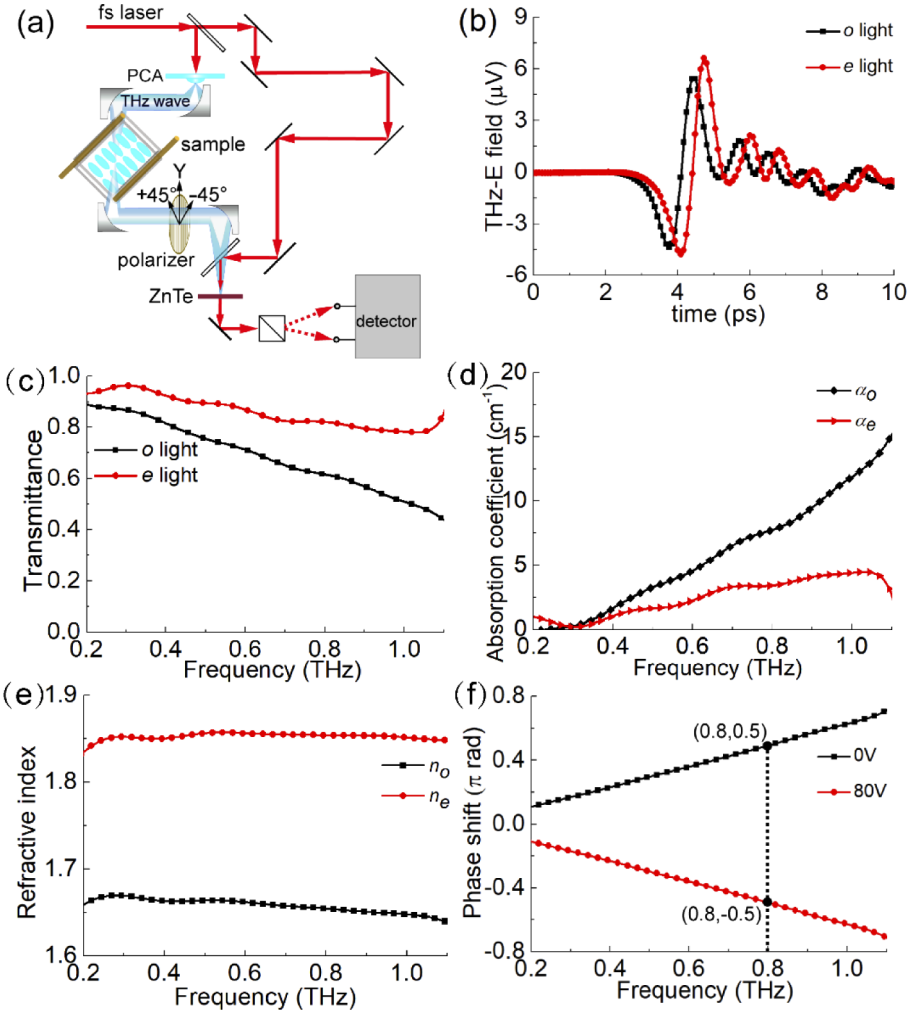

Fig. 2. THz-TDS system and experimental results of PDLC. (a) The THz-TDS system light path diagram; (b) The time domain signals of *o*-light and *e*-light; (c) The intensity transmittances and (d) absorption coefficients of *o*-light and *e*-light; (e) The refractive index n_o and n_e of PDLC; (f) Phase shifts of PDLC layer with the thickness of 500 μm under 0 V and 80 V.

Optical Materials EXPRESS

in Fig. 2(e), n_o and n_e are about 1.65 and 1.85 with a slight dispersion in the broadband THz frequency range, respectively.

In the second step of the experiment, we further investigated the PDLC cell used as a THz electrically tunable phase shifter. In this case, the PDLC cell was rotated to θ=+45° as shown in Fig. 2(a). We can rotate the THz polarizer at + 45° and -45° to measure the two orthogonal LP components of output light passing through the PDLC cell. The birefringence phase shift of the LC cell can be obtained, which is exhibited in Fig. 2(f). When there is no DC voltage applied between the two electrodes of the PDLC cell, the optical axis of the PDLC is along θ=+45° direction. In this case, the phase shift of the LC cell is positive, linearly increasing with the growing frequency and exactly reaching 0.5π at 0.8 THz, which means that the LC cell realizes the function as a quarter-wave plate at 0.8 THz. When the DC voltage gradually increases to 80 V, the optical axis of the PDLC turns to the θ=−45° direction. The phase shift curve is reversed to be negative in this case, exactly obtaining -0.5π at 0.8 THz, which means that the LC cell in this situation also serves as a quarter-wave plate. As a result, the pure PDLC cell can be used as a quarter-wave plate with an adjustable optical axis at 0.8 THz, just realizing the conversion from a LP light to a circularly polarized (CP) light. However, a higher frequency is required to obtain a wider phase shift range.

2.2. Artificial birefringence of dielectric grating

We consider using a Si grating to introduce high THz artificial birefringence, of which the anisotropy mechanism originates from the difference in the filling rate of the Si between along and perpendicular to the grating grid direction. The refractive index of Si is 3.42 in the THz regime with a negligible absorption loss. The equivalent refractive index perpendicular to the grid direction will be much smaller than that of silicon due to the periodic modulation of air/silicon structure according to the equivalent medium theory. Different from the ordinary gratings with the fixed grating grid, we designed a gradient grating with multiple gradient grids in a super cell, so that this grating can manipulate the dispersion characteristic of PDLC. As shown in Fig. 3(a), this dielectric grating has 10 ridges and 10 grooves in one period, where the ridge width is invariably 60 μm, but the groove width is gradually varied, increasing from the minimum groove width of 15 μm to the maximum one of 60 μm with the gradient of 5 μm. The etched depth is 200 μm, and the silicon substrate thickness is 300 μm. The microscope photograph of the grating is shown in Fig. 3(b). The dielectric grating was fabricated by the silicon deep etching technology in micro-electromechanical systems (MEMS). Firstly, a 500 μm thickness Si wafer with a high resistivity of 10 KΩ · cm is cleaned, and a 5 μm photoresist layer is spun onto the wafer. Then, exposed by UV light through a designed mask, the wafer will generate the expected structure, and finally the wafer is shaped by the inductively coupled plasma etching. The different etching time is required for the different etching depth, about 70 mins for 200 μm. The size of the whole grating sample is 1 cm × 1 cm.

We also measured the birefringence and phase shift of this dielectric grating by using the THz-TDS system, and the results are presented in Figs. 3(c) and 3(d), respectively. The refractive index along the ridge direction of grating is defined as n_e, which is larger than the refractive index n_o along the orientation perpendicular to the ridge direction, therefore the direction along the ridge of grating is defined as the long axis of this birefringent grating. Different from the refractive index of PDLC, both the refractive index n_e and n_o of the dielectric grating exhibit a significant dispersion. And the birefringence ($\Delta n = n_e - n_o$) decreases with the increasing frequency (*i.e.* negative dispersion), so that the phase shift spectrum in Fig. 3(d) is a flat curve close to π in the wide band from 0.55 to 1.05 THz, that is to say, realizing the function as an achromatic wave plate in a broad band range.

Optical Materials EXPRESS

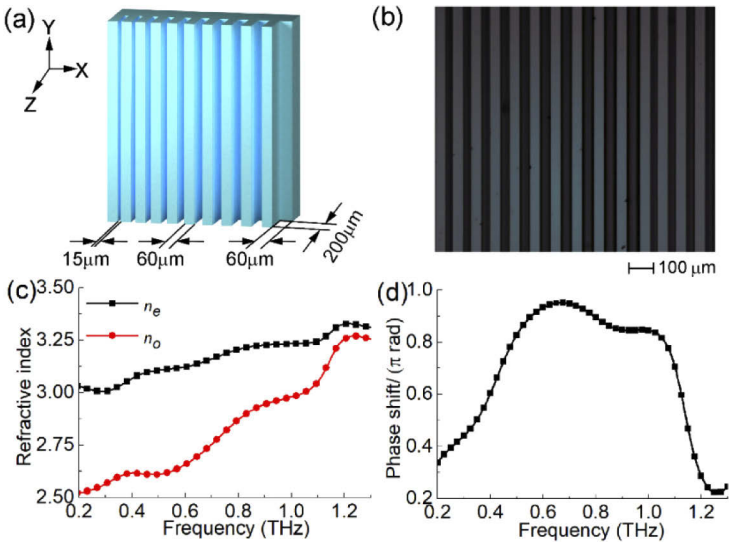

Fig. 3. Geometric structure and birefringence properties of the dielectric gradient grating. (a) Structure diagram of the grating; (b) Microscope photograph of the grating; (c) Experimental refractive index n_o and n_e of the grating; (d) Experimental birefringence phase shift of the grating.

2.3. Design of phase shifter based on the birefringence grating filled with PDLC

From the results above, we can see that the PDLC is an adjustable natural birefringent material, of which the optical axis can rotate with the biased electric field, and the dielectric gradient grating is an artificial birefringence material with a fixed optical axis, which can function as a broadband achromatic waveplate. Therefore, we consider filling PDLCs into the surface of the dielectric grating by an appropriate design, so that the tunable phase shift range and dispersion of PDLC can be improved. As shown in Fig. 4(a), without biased electric field, the LC molecules are aligned along the ridge direction of grating (θ=90°). In this case, the optical axis direction of LCs and dielectric grating is the same, so that the total birefringence of this device is enhanced, therefore obtaining the maximum phase shift. After applying a DC electric field along x axis, the LC molecules gradually rotate to the x axis as shown in Fig. 4(b), and when the applied DC voltage reaches 80 V, finally the optical axis of LCs is along the electric field direction (θ=0°), vertical to the optical axis of the grating. That is to say, by adjusting the thickness of PDLC layer, the birefringence of the LC and dielectric grating can exactly offset each other so that this device reaches an isotropic state without birefringence phase shift. As a result, the phase shift of this device can be tuned between 0° and the maximum value, improving the maximum tunable range of the LC device, compared with a similar thickness of LC layer discussed in Section 2.1.

We simulated the results of this device in the commercial software CST Studio. The simulation parameters of PDLC, such as the thickness of PDLC layer, the refractive index n_o and n_e of PDLC without considering the loss of PDLC, are followed with Section 2.1. The simulation parameters of the dielectric grating are configured as Section 2.2, and the grating direction is along y axis. The x and y directions are set as the periodic boundary condition, and an open boundary condition is set in the z direction. As a light source, the 45° LP light is incident along z axis to get the same x and y components.

As shown in Fig. 4(c), the phase shift of this device decreases with the decreasing θ from 90° to 0°, namely the PDLC molecules rotating from y axis to x axis. At 0.375 THz, when θ is 0° and 90°, the corresponding phase shifts are 0.06π and 0.56π, respectively, namely with the phase modulation depth of 0.5π at 0.375 THz. When $\theta = 0°$ and 90°, the phase shifts reach 0 and π at

Optical Materials EXPRESS

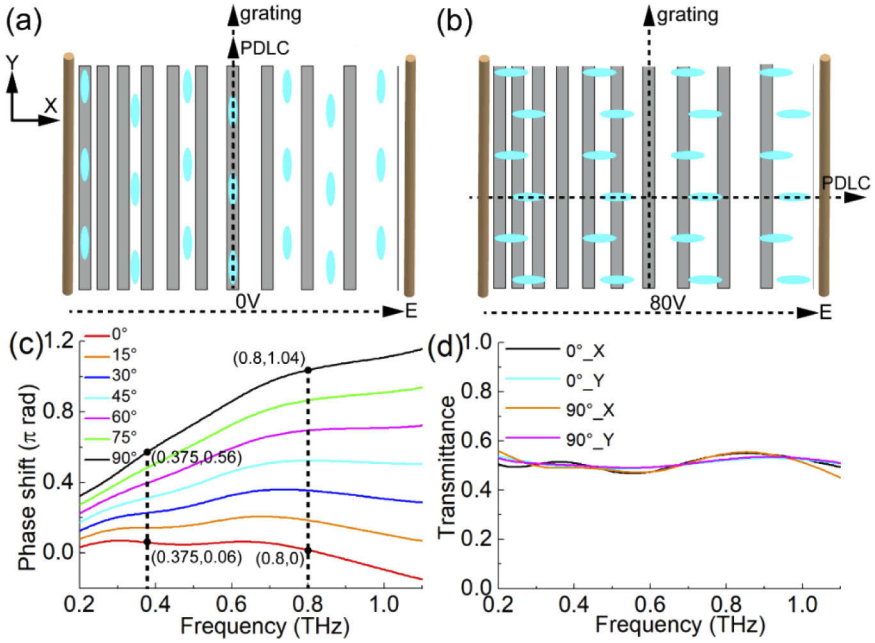

Fig. 4. Schematic diagrams and simulation results of the dielectric gradient grating filled with PDLCs. (a) Schematic that the orientation of PDLC molecules is parallel with the grating direction when $E = 0$ V; (b) Schematic in which the orientation of PDLC molecules is perpendicular with the grating direction when $E = 80$ V; (c) Simulative phase shifts when the orientation of PDLC molecules gradually rotate from y axis (θ=90°) to x axis (θ=0°), representing the process of the increasing voltage from 0 V to 80 V; (d) Simulative intensity transmittances of x and y components when θ is 0° and 90°, respectively.

0.8 THz, respectively, namely with the phase modulation depth of π at 0.8 THz. That is to say, compared with the tunable phase shift range of pure PDLC cell from -0.5π to 0.5π at 0.8 THz in Section 2.1, the introduction of the dielectric grating improves the tunable range from 0 to π at 0.8 THz. Moreover, owing to the dispersion control of the gradient grating, the phase shift curve of this device becomes flatter than that of the pure PDLC cell. Furthermore, the simulative transmissions of x and y components at θ=0° and 90° are shown in Fig. 4(d), which shows the intensity transmittance of the two orthogonal components is basically the same about 50%, and there is no resonance peak in the broad THz band from 0.2 to 1.1 THz.

With the amplitudes of the two orthogonal LP components (A_x and A_y) and the phase shifts between them ($\Delta\delta$), we can reconstruct the polarization ellipse of the output light. Figures 5(a) and 5(b) show the polarization ellipse at 0.375 THz and 0.8 THz obtained by

$$\frac{{E_x}^2}{{A_x}^2} + \frac{{E_y}^2}{{A_y}^2} - \frac{2E_xE_y}{A_xA_y}\cos\Delta\delta = \sin^2\Delta\delta \tag{4}$$

Two important polarization parameters, the elliptic angle χ and the polarization rotating angle φ, are respectively defined by

$$\tan 2\chi = \sin 2\beta \sin\Delta\delta \tag{5}$$

$$\tan 2\varphi = \tan 2\beta \cos\Delta\delta \tag{6}$$

where $\tan\beta = A_y/A_x$. If χ=45°, the polarization state is a CP. On the contrary, if χ is 0°, the polarization state is a LP. In Fig. 5(a), the polarization state of the output light at 0.375 THz transforms from the initial LP along the y axis, gradually to the elliptical polarizations, and finally

Optical Materials EXPRESS

to the CP, demonstrating that this device can function as a tunable quarter-wave plate at 0.375 THz. Figure 5(b) shows that the polarization state of the output light at 0.8 THz converts from the original LP along with the *y* axis, gradually to the CP, and eventually to the LP orthogonal with the initial LP, proving that this device can act as an adjustable half-wave plate at 0.8 THz.

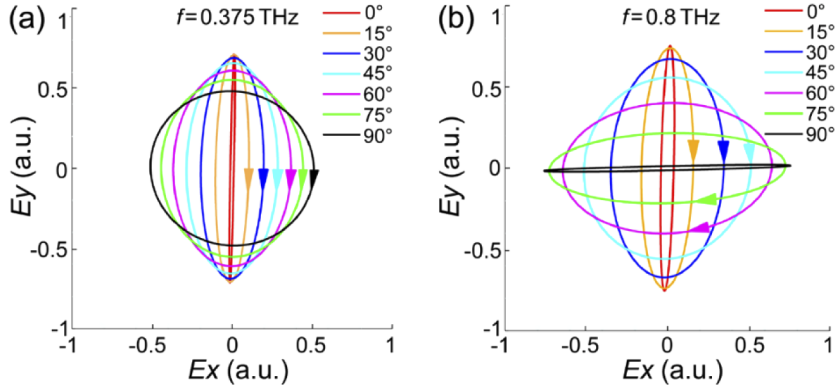

Fig. 5. Simulative polarization states of dielectric gradient grating filled with PDLC under the different LC molecular orientation angles. (a) At 0.375 THz; (b) At 0.8 THz.

2.4. *Experiment of phase shifter based on the birefringence grating filled with PDLC*

At last, we experimentally confirmed the proposed device. The LC cell used in the experiment is shown in Fig. 6(a), which is still encased in two pieces of quartz glass. The PDLC layer is just on the surface of the dielectric grating and between the two copper wires, and the grooves

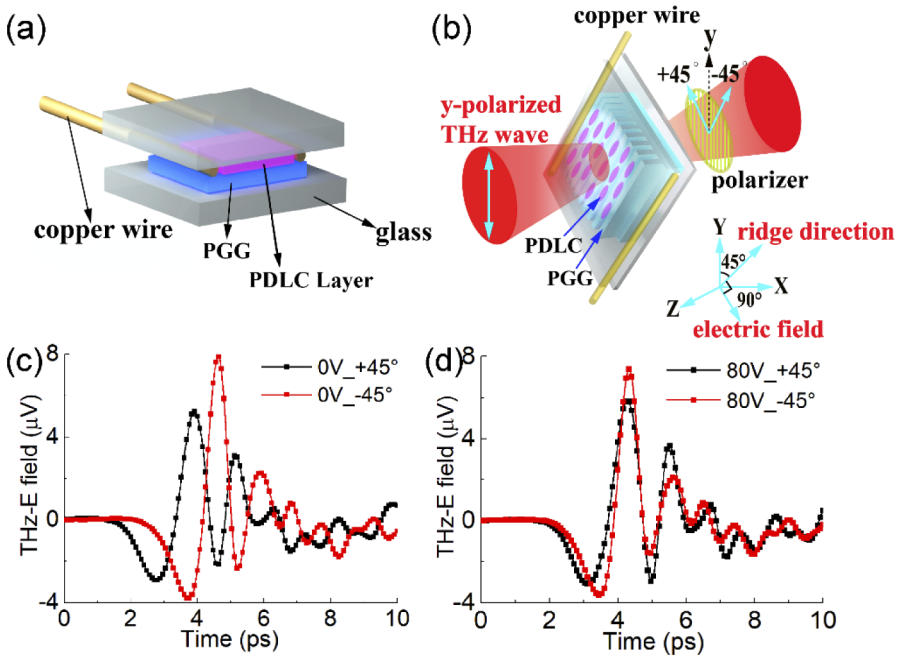

Fig. 6. Schematic diagram in the experiment and experimental data. (a) The structure of the dielectric gradient grating filled with PDLCs in the experiment; (b) The schematic diagram of geometry configuration in the measurement; (c) The time domain signals of + 45° and -45° LP components at 0 V and (d) 80 V measured by THz-TDS system, respectively.

Optical Materials EXPRESS

of the grating are filled with PDLCs. The edge parts between the two pieces of glass are filled by solidified UV glue to wrap the grating and the PDLC layer so that forming the LC cell of a sealed structure. The experimental light path is shown in Fig. 6(b), where the grating direction forms an angle of 45° to the *y* axis, and the biased DC electric field is perpendicular with the grating direction. The PDLC molecules are initially anchored by an external magnetic field and UV light, which are aligned along the grating direction. With the increasing voltage from 0 V to 80 V, the PDLC molecules gradually rotate perpendicular to the grating direction.

The time domain signals of + 45° and -45° components at $E = 0$ V and 80 V are measured. When $E = 0$ V, the birefringence of the grating and the PDLC is superposed, and the optical axis of the device is along the -45° direction, exhibiting an anisotropic state. As shown in Fig. 6(c), the two signals are very different, almost the peak corresponding to the valley, which means they are nearly reversed 180°. While when $E = 80$ V, the birefringence of the grating offsets the one of PDLC, and meantime the device is isotropic. As shown in Fig. 6(d), the two signals become almost overlapped, which means no delay in the phase shift. Furthermore, the intensity transmittances of + 45° and -45° LP components at 0 V and 80 V are exhibited in Fig. 7(a) and 7(b), respectively. When $E = 0$ V, the transmittance of the -45° LP component along the optical axis is greater than that of the + 45° LP component perpendicular to the optical axis, which is mainly due to the different absorption of the PDLC along the two orthogonal directions. At this time, the total intensity transmittance of the device at 0.8 THz is 52% and the insertion loss is -2.83 dB. When $E = 80$ V, the whole structure is in isotropic state, thus the transmittances of the -45° and + 45° LP components are similar. In this case, the total intensity transmittance of the device at 0.8 THz is 49% and the loss is -3.09 dB.

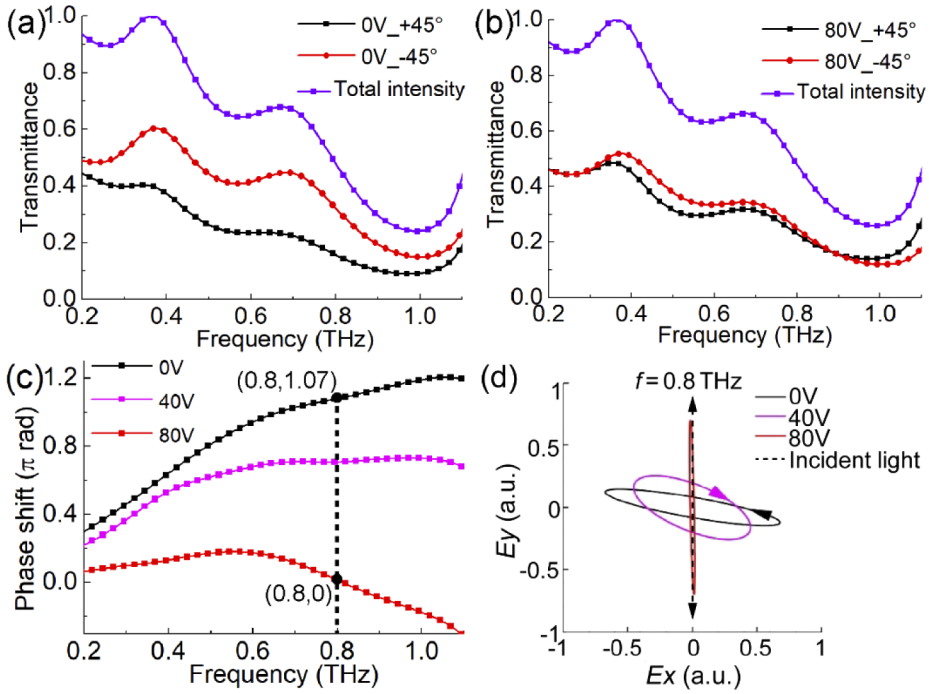

Fig. 7. Experimental results of the dielectric gradient grating filled with PDLCs. (a) The intensity transmittances of + 45° and -45° LP components at 0 V and (b) 80 V; (c) The curves of birefringent phase shift at 0 V, 40 V and 80 V; (d) Polarization ellipses when $E = 0$ V, 40 V and 80 V at 0.8 THz.

Optical Materials EXPRESS

The phase shifts at 0 V, 40 V and 80 V are presented in Fig. 7(c), and these experimental curves are consistent with those of simulation shown in Fig. 4(c). At 0.8 THz, the phase shift reaches 1.07π rad at 0 V, and it becomes 0 when the voltage is increased to 80 V. The tunable range of phase shift is basically from 0 to π at 0.8 THz. Besides, the polarization ellipses can be calculated by Eq. (4) shown in Fig. 7(d). When the incident light is *y*-LP, the polarization state of output light at 0.8 THz is the initial left-handed CP light with the elliptic angle of -6.55° and polarization rotating angle of 79.62° at 0 V (*i.e.* close to a *x*-LP, the device realizes the function of orthogonal polarization conversion as a half-wave plate). Then it becomes the right-handed elliptical polarized state, and finally to the *y*-LP with the elliptic angle of 1.27° and polarization rotating angle of 1.17° (*i.e.* the function of orthogonal polarization conversion is OFF). The main reason why the polarization state at 0 V is not a strictly orthogonal LP light is that the phase shift is 1.07π not just π rad and the transmittances of the two orthogonal LP components are not strictly same. To sum up, the experimental results basically fit with our design discussed above.

3. Conclusion

In summary, we present a new active manipulation mechanism of THz anisotropy based on a dielectric gradient grating filled with PDLC. Here, PDLC serves as a tunable anisotropic material based on the rotation of LC molecular orientation caused by the biased electric field, while the grating acts as an artificial high birefringence material with a fixed optical axis. By filling PDLC into the surface of the grating, the superposition of two birefringence effects makes the anisotropy of the total structure enhanced or eliminated, and the dispersion of phase shift curve is engineered to be smaller in the broad THz frequency range. This designing manipulates the phase shift of this structure changes from π to 0 around 0.8 THz when the electric field is applied from 0 to 80 V. The experiment results support the simulation design of this device, which implements the tunable polarization transformation function of THz half-wave plate. This work that combined with LC and artificial microstructure will bring new ideas for researches in developing active THz phase and polarization devices.

Funding

National Key Research and Development Program of China (2017YFA0701000); National Natural Science Foundation of China (61831012, 61971242); Natural Science Foundation of Tianjin City (19JCYBJC16600); Young Elite Scientists Sponsorship Program by Tianjin (TJSQNTJ-2017-12).

Disclosures

The authors declare that there are no conflicts of interest related to this article.

References

1. Y. X. Fan, Y. X. Qian, S. Yin, D. X. Li, M. Z. Jiang, X. Lin, and F. R. Hu, "Multi-band tunable terahertz bandpass filter based on vanadium dioxide hybrid metamaterial," Mater. Res. Express **6**(5), 055809 (2019).
2. S. Chen, F. Fan, Y. Miao, X. He, K. Zhang, and S. Chang, "Ultrasensitive terahertz modulation by silicon-grown MoS2 nanosheets," Nanoscale **8**(8), 4713–4719 (2016).
3. Y. Y. Ji, F. Fan, X. H. Wang, and S. J. Chang, "Broadband controllable terahertz quarter-wave plate based on graphene gratings with liquid crystals," Opt. Express **26**(10), 12852–12862 (2018).
4. Y. Z. Cheng, W. Withayachumnankul, A. Upadhyay, D. Headland, Y. Nie, R. Z. Gong, M. Bhaskaran, S. Sriram, and D. Abbott, "Ultrabroadband reflective polarization convertor for terahertz waves," Appl. Phys. Lett. **105**(18), 181111 (2014).
5. T. Kleine-Ostmann and T. Nagatsuma, "A Review on Terahertz Communications Research," J. Infrared, Millimeter, Terahertz Waves **32**(2), 143–171 (2011).
6. P. U. Jepsen, D. G. Cooke, and M. Koch, "Terahertz spectroscopy and imaging - Modern techniques and applications," Laser Photonics Rev. **5**(1), 124–166 (2011).
7. T. Chen, S. Li, and H. Sun, "Metamaterials application in sensing," Sensors **12**(3), 2742–2765 (2012).

Optical Materials EXPRESS

8. D. C. Wang, Y. H. Gu, Y. D. Gong, C. W. Qiu, and M. H. Hong, "An ultrathin terahertz quarter-wave plate using planar babinet-inverted metasurface," Opt. Express **23**(9), 11114–11122 (2015).
9. X. M. Ke, H. Zhu, J. H. Li, L. Chen, and X. Li, "Double-stacked hyperbolic metamaterial waveguide arrays for efficient and broadband terahertz quarter-wave plates," Sci. Rep. **7**(1), 574 (2017).
10. Z. L. Han, S. Ohno, Y. Tokizane, K. Nawata, T. Notake, Y. Takida, and H. Minamide, "Off-resonance and in-resonance metamaterial design for a high-transmission terahertz-wave quarter-wave plate," Opt. Lett. **43**(12), 2977–2980 (2018).
11. T. R. Tsai, C. Y. Chen, C. L. Pan, R. P. Pan, and X. C. Zhang, "Terahertz time-domain spectroscopy studies of the optical constants of the nematic liquid crystal 5CB," Appl. Opt. **42**(13), 2372–2376 (2003).
12. C.-F. Hsieh, C.-S. Yang, F.-C. Shih, R.-P. Pan, and C.-L. Pan, "Liquid-crystal-based magnetically tunable terahertz achromatic quarter-wave plate," Opt. Express **27**(7), 9933–9940 (2019).
13. L. Wang, X. W. Lin, X. Liang, J. B. Wu, W. Hu, Z. G. Zheng, B. B. Jin, Y. Q. Qin, and Y. Q. Lu, "Large birefringence liquid crystal material in terahertz range," Opt. Mater. Express **2**(10), 1314–1319 (2012).
14. R. Kowerdziej, M. Olifierczuk, and J. Parka, "Thermally induced tunability of a terahertz metamaterial by using a specially designed nematic liquid crystal mixture," Opt. Express **26**(3), 2443–2452 (2018).
15. B. Vasic, D. C. Zografopoulos, G. Isic, R. Beccherelli, and R. Gajic, "Electrically tunable terahertz polarization converter based on overcoupled metal-isolator-metal metamaterials infiltrated with liquid crystals," Nanotechnology **28**(12), 124002 (2017).
16. Y. Ji, F. Fan, S. Xu, J. Yu, and S. Chang, "Manipulation enhancement of terahertz liquid crystal phase shifter magnetically induced by ferromagnetic nanoparticles," Nanoscale **11**(11), 4933–4941 (2019).
17. N. Vieweg, C. Jansen, M. K. Shakfa, M. Scheller, N. Krumbholz, R. Wilk, M. Mikulics, and M. Koch, "Molecular properties of liquid crystals in the terahertz frequency range," Opt. Express **18**(6), 6097–6107 (2010).
18. L. Yang, F. Fan, M. Chen, X. Z. Zhang, J. J. Bai, and S. J. Chang, "Magnetically induced birefringence of randomly aligned liquid crystals in the terahertz regime under a weak magnetic field," Opt. Mater. Express **6**(9), 2803 (2016).
19. S. Harbour, J. V. Kelly, T. Galstian, and J. T. Sheridan, "Optical birefringence and anisotropic scattering in acrylate based holographic polymer dispersed liquid crystals," Opt. Commun. **278**(1), 28–33 (2007).
20. Y. Inoue, H. Kubo, T. Shikada, and H. Moritake, "Ideal Polymer-LC Composite Structure for Terahertz Phase Shifters," Macromol. Mater. Eng. **304**(4), 1800766 (2019).
21. C. L. Chang, W. C. Wang, H. R. Lin, F. J. Hsieh, Y. B. Pun, and C. H. Chan, "Tunable terahertz fishnet metamaterial," Appl. Phys. Lett. **102**(15), 151903 (2013).
22. R. Kowerdziej, M. Olifierczuk, J. Parka, and J. Wrobel, "Terahertz characterization of tunable metamaterial based on electrically controlled nematic liquid crystal," Appl. Phys. Lett. **105**(2), 022908 (2014).
23. C. S. Yang, T. T. Tang, P. H. Chen, R. P. Pan, P. S. Yu, and C. L. Pan, "Voltage-controlled liquid-crystal terahertz phase shifter with indium-tin-oxide nanowhiskers as transparent electrodes," Opt. Lett. **39**(8), 2511–2513 (2014).
24. M. P. Hokmabadi, A. Tareki, E. Rivera, P. Kung, R. G. Lindquist, and S. M. Kim, "Investigation of tunable terahertz metamaterial perfect absorber with anisotropic dielectric liquid crystal," AIP Adv. **7**(1), 015102 (2017).
25. O. Buchnev, N. Podoliak, M. Kaczmarek, N. I. Zheludev, and V. A. Fedotov, "Electrically Controlled Nanostructured Metasurface Loaded with Liquid Crystal: Toward Multifunctional Photonic Switch," Adv. Opt. Mater. **3**(5), 674–679 (2015).
26. T. Sasaki, H. Kushida, M. Sakamoto, K. Noda, H. Okamoto, N. Kawatsuki, and H. Ono, "Liquid crystal cells with subwavelength metallic gratings for transmissive terahertz elements with electrical tunability," Opt. Commun. **431**, 63–67 (2019).
27. J. Wang, H. Tian, Y. Wang, X. Y. Li, Y. J. Cao, L. Li, J. L. Liu, and Z. X. Zhou, "Liquid crystal terahertz modulator with plasmon-induced transparency metamaterial," Opt. Express **26**(5), 5769–5776 (2018).
28. L. Wang, S. J. Ge, W. Hu, M. Nakajima, and Y. Q. Lu, "Graphene-assisted high-efficiency liquid crystal tunable terahertz metamaterial absorber," Opt. Express **25**(20), 23873–23879 (2017).
29. L. Wang, X. W. Lin, W. Hu, G. H. Shao, P. Chen, L. J. Liang, B. B. Jin, P. H. Wu, H. Qian, Y. N. Lu, X. Liang, Z. G. Zheng, and Y. Q. Lu, "Broadband tunable liquid crystal terahertz waveplates driven with porous graphene electrodes," Light: Sci. Appl. **4**(2), e253 (2015).
30. J. Yang, P. Wang, T. Shi, S. Gao, H. B. Lu, Z. P. Yin, W. E. Lai, and G. S. Deng, "Electrically tunable liquid crystal terahertz device based on double-layer plasmonic metamaterial," Opt. Express **27**(19), 27039–27045 (2019).
31. X. F. Li, N. Tan, M. Pivnenko, J. Sibik, J. A. Zeitler, and D. P. Chu, "High-birefringence nematic liquid crystal for broadband THz applications," Liq. Cryst. **43**(7), 955–962 (2016).